Study on the desorption of CO_2 from MEA aqueous solution over iron-titanium mixed oxide catalyst synthesized by microwave irradiation treatment

Mengyao Wang[1], Yanping Du[2], Haoran Zhang[1], Junge Lv[1], Huancong Shi[1], Wei Lu[1], Jing Jin[1,3], Zhibo Xiong[1]*

1. School of Energy and Power Engineering, University of Shanghai for Science & Technology, Shanghai, 200093, China

2. School of Engineering, Lancaster University, Lancaster, LA1 4YW, UK

3. Shanghai Non-carbon Energy Conversion and Utilization Institute, Shanghai 200240, China

Abstract: The energy-intensive regeneration of amine-based solvents remains a major bottleneck in CO_2 capture from fossil-fuel combustion flue, which is due to the high thermal consumption and slow desorption kinetics. To address these challenges, this study aims to develop a cost-effective, high-performance solid-acid catalyst to accelerate CO_2 desorption from CO_2-rich monoethanolamine (MEA) solutions while reducing energy input. A series of $FeTiO_x$-M catalysts were synthesized via a microwave-assisting co-precipitation method and the as-prepared catalysts were characterized by XRD, FT-IR, Py-IR, XPS, NH_3-TPD, and N_2 adsorption-desorption to elucidate structure-activity relationships. Results indicate that the $Fe_{25}Ti_{75}O_x$-M catalyst achieves a 36% increase in the average CO_2 desorption rate and a 25.7% reduction in relative heat duty at 0.4 wt. % loading and 90 °C, with certain stable activity maintained over five cycles. The enhanced performance is attributed to synergistic combination of abundant Brønsted and Lewis acid sites, activated surface hydroxyls by sulfate groups, and enlarged mesoporous surface area that facilitates carbamate diffusion. These findings demonstrate that rational design of bimetallic solid-acid catalysts can substantially improve CO_2 desorption efficiency and energy savings, therefore providing a scalable and energy-efficient strategy for amine regeneration in industrial-level CO_2 capture applications.

Keywords: CO_2 desorption, MEA, Iron-titanium oxide, Acid site, Mesoporous structure

* Corresponding author: Zhibo Xiong, Tel.: +86 21 55272320, Email addresses: xzb412@usst.edu.cn (Zhibo Xiong)

1. Introduction

Global energy demand is continuously rising with the rapid development of the global economy [1]. This trend is further intensified by the slow deployment of low-emission technologies and the continuing heavy reliance on fossil-fuel combustion [2,3]. Consequently, the dramatic increase in emissions of carbon dioxide and other greenhouse gases has made global warming severe challenge to human survival and development [4,5]. Carbon Capture, Utilization and Storage (CCUS) is recognized as a critical technology for achieving net-zero carbon emissions from fossil energy and one of the most viable solutions for limiting atmospheric CO_2 releases, with its core objective being to facilitate the transition toward net-zero CO_2 emissions [6,7].

Currently, CO_2 capture technologies are primarily categorized into pre-combustion decarbonization, in-combustion CO_2 capture, and post-combustion CO_2 capture, based on the integrated position and circulation of the CO_2 separation process within the power system [8,9]. Chemical absorption is currently one of the most promising and widely applied technologies for CO_2 capture due to its high efficiency, mature process, and strong adaptability to existing industrial systems. It offers high selectivity and large absorption capacity, especially when using amine-based solvents. Compared to other methods, chemical absorption has rich engineering experience and is relatively easy to scale up. However, it suffers from high regeneration energy consumption, equipment corrosion, and solvent degradation, which significantly limit its large-scale deployment [10-12]. Based on this, researchers have conducted extensive research efforts to accelerate CO_2 desorption from amine solvents while simultaneously reducing regeneration energy consumption. For instance, recent studies have achieved notable progress in lowering regeneration energy through the development of biphasic absorbents [13] and blended primary amine systems [14,15]. Nevertheless, inherent limitations remain for absorbent modification alone. As the current benchmark solvent for amine scrubbing, the 30 wt.% MEA aqueous solution exhibits an actual regeneration energy consumption exceeding the theoretical minimum by 0.93 GJ/t·CO_2 [16-18], demonstrating substantial optimization potential in thermal desorption regeneration. Additionally, this system experiences volatile amine losses with associated carcinogenic risks [19]. While elevated temperature and reduced pressure enhance CO_2 desorption rates, employing tailored heterogeneous catalysts proves to be more effective in balancing high desorption kinetics with low regeneration energy consumption [20,21].

In recent years, the application of solid acid catalysts (SACs) has emerged as a promising strategy to reduce energy requirement and increase CO_2 desorption capacity for the regeneration of MEA solvent [22,23]. Using solid acid catalysts for CO_2 desorption can reduce the energy barriers related to the C-N bond breaking in carbamate and speed up the proton transfer rate in protonated amines [24]. Metal oxides are typical SACs, offering simple preparation routes, low cost, and robust catalytic activity [25]. Li et al. [26] fabricated a solid-acid catalyst by one-step urea-hydrolysis of sepiolite (SEP) to anchor SO_4^{2-}/ZrO_2 (SZ), yielding SZ@SEP composites with tunable SZ/SEP ratios. Among them, SZ@SEP-1/2 exhibited the highest density of Brønsted and Lewis acid sites. When 2 g of SZ@SEP-1/2 was suspended in 5 M MEA at 88 °C, the CO_2 desorption rate rose by 92 % and the relative heat duty dropped by 48.6 % versus blank thermal regeneration, and the catalyst retained stable activity over 20 cycles, confirming its potential for energy-efficient CO_2 capture. Rao et al. [27] prepared a ternary Fe/SiO_2/biochar solid-acid catalyst via one-pot pyrolysis of wheat flour, SiO_2 and $FeCl_3$. In 30 wt. % MEA at 90 °C the best sample (FSC_2) raised the CO_2 desorption amount by 35 % and cut the relative heat duty by 34 % versus blank thermal regeneration, and activity loss after five cycles was only 6.1 %. The performance gain is ascribed to abundant Brønsted/Lewis acid sites and a reversible Fe (II)/Fe (III) redox couple that jointly accelerate carbamate/bicarbonate cleavage and proton transfer, offering an energy-efficient and stable route for amine solvent regeneration. Jin et al. [28] prepared black TiO_2 nanoparticles by $NaBH_4$ reduction of P25, and the resulting material functions simultaneously as a photothermal converter and a solid-acid catalyst. Surface bridging hydroxyls supply Brønsted acid sites, while Ti^{3+}/Ti^{4+} centers act as Lewis acid sites, accelerating carbamate and bicarbonate decomposition during CO_2 desorption from MEA solution at ≈ 88 °C under 7-sun irradiation. The above results indicate that nanostructured SACs can significantly improve the absorption and desorption performance of the system [29]. In addition, some metal-organic framework-based solid acid catalysts have been reported for CO_2 desorption processes due to their advantages of high porosity, selectivity, flexible structure, and ease of modification/functionalization [30,31]. However, their industrial application is limited by either high production cost or insufficient catalytic efficiency. Therefore, it is of significance to develop cost-effective and highly active solid acid catalysts that are inexpensive yet highly effective for promoting the regeneration of amine-rich solutions [32].

Studies had shown that metal-oxide nanoparticles combine physical and chemical promotion,

and they physically broke bubbles via Brownian motion, enlarged the interfacial area and lowered mass-transfer resistance, while their surfaces abound in Lewis and Brønsted acid sites helped to promote CO_2 reactions, leading to markedly higher CO_2-desorption rates [33,34]. However, their modest specific surface area, irregular pore size and rapid deactivation limit their use at high temperatures and in aqueous amine systems [35]. Relative to single-metal ions, the differing electron affinities of elements in mixed-metal oxides strongly alter the electronic coordination environment around multiple metal ions [36]. Among the reported candidates, iron-based catalysts had been identified as exceptionally efficient for CO_2-catalyzed desorption, benefiting from their abundant acidic sites and the facile electron transfer mediated by the Fe(II)/Fe(III) redox cycle [27]. On the other hand, our research group had demonstrated the catalytic promotion of microwave-irradiated FeOOH catalysts for the regeneration of CO_2-rich MEA solutions, highlighting the significant impact of a large specific surface area and abundant Lewis acid sites on catalytic performance. Ti^{4+} (74.5 pm) has been shown to be a promising dopant due to its ionic radius being comparable to that of Fe^{3+} (69 pm) and its half-filled (d^5) electron configuration [37]. And in the study by Jiang et al. [38], the improvement of the absorption properties of MEA and MDEA solutions by different nanoparticles was examined. The findings indicated that TiO_2 particles exhibited the most significant enhancement factor, followed by MgO with Al_2O_3, and SiO_2 particles demonstrated the least enhancement. Additionally, Geng [39] et al. systematically demonstrated the significant catalytic effect of a mesoporous, high-acid-density SO_4^{2-}/ZrTiO*x* solid acid catalyst on CO_2 desorption in a 90 °C, 5 mol MEA system. In this study, metal-element doping was employed to mitigate mesopore collapse induced by high-temperature calcination, while dual active sites were introduced to synergistically accelerate CO_2 desorption from amine-rich solutions.

Microwave irradiation enables rapid and uniform heating of the reaction medium, inducing an explosive surge in nucleation that favors products with small particle sizes and narrow size distributions [40,41]. On the other hand, the volumetric heating characteristic of microwaves allows the interior of the adsorbent to heat up instantly, markedly shortening CO_2 desorption time, lowering regeneration energy consumption, and improving microwave energy utilization efficiency-an advantage that also applies to catalysts [42,43]. Therefore, microwave irradiation treatment is expected to refine the particle size of Fe-Ti composite catalysts, enlarge their specific surface area and acid-site density, and consequently enhance their performance for CO_2 desorption from MEA solution.

In this study, a series of $FeTiO_z$-M-20 catalysts were prepared by a co-precipitation-microwave method to evaluate their performance in CO_2 desorption from CO_2-rich MEA solutions. Five catalysts with different Fe^{3+}:Ti^{4+} molar ratios-0:100, 25:75, 50:50, 75:25 and 100:0, were investigated. In addition, the catalyst exhibiting the highest activity was further subjected to five absorption–desorption cycles to examine its stability and potential influence on subsequent CO_2 absorption. Comprehensive physicochemical characterization, including XRD, FT-IR, Py-IR, XPS, and NH_3-TPD, was performed to elucidate the structure-activity relationships on governing the catalytic behavior.

2. Experimental

2.1 Catalyst preparation

All reagents were of analytical grade (AR) and used directly without further purification. Initially, predetermined amounts of $Fe(NO_3)_3 \cdot 9H_2O$ and $Ti(SO_4)_2 \cdot 7H_2O$ were dissolved in 150 mL of deionized water and vigorously stirred for 1 h. Subsequently, 2 mol/L $NH_3 \cdot H_2O$ was added dropwise into the mixed solution until the pH reached 9-10. The resulting suspension was then immediately filtered without an aging step and thoroughly washed. The obtained wet precipitate was subjected to microwave irradiation at power level P_{30} for 20 min using a domestic microwave oven (EG823MF3-NW, Midea, China), followed by calcination in static air at 400 °C for 5 h to yield the final catalysts. These materials were denoted as $Fe_xTi_{100-x}O_z$-M, where x represents the molar ratio of $Fe^{3+}/(Fe^{3+}+Ti^{4+})$ in the precursor solution prior to the titration and precipitation. Five catalysts were prepared analogously and labeled as TiO_2-M, $Fe_{25}Ti_{75}O_z$-M, $Fe_{50}Ti_{50}O_z$-M, $Fe_{75}Ti_{25}O_z$-M and Fe_2O_3-M, respectively.

2.2 Catalytic activity Test

X-ray diffraction (XRD) patterns were collected on a Rigaku Smart Lab diffractometer (Japan Science) using Cu Kα radiation (λ = 0.15406 nm) over 2θ = 20-80 ° at a scan speed of 2 °/min under 40 kV and 40 mA. N_2 adsorption-desorption isotherms were acquired with a Micromeritics ASAP 2460 analyzer at 77 K, and specific surface areas and pore-size distributions are obtained through Brunauer-Emmett-Teller (BET) calculations and Barrett-Joyner-Halenda (BJH). X-ray photoelectron spectroscopy (XPS) was performed on a Thermo-Fisher Scientific Escalab 250 Xi (USA) with 150 W monochromated Al Kα radiation (1486.6 eV). Binding energies of Fe 2p and O 1s were referenced to the C 1s peak at 284.8 eV. Fourier-transform infrared spectra (FTIR) were

recorded on a Nicolet iS5 spectrometer (4 cm^{-1} resolution) from 400 to 4000 cm^{-1}. Acid-site characterization by pyridine-IR (Py-IR) was carried out via a Thermo Nicolet 380 spectrometer. Samples were firstly evacuated at 105 °C, cooled to ambient temperature, and then exposed to a 20 mL/min He flow saturated with pyridine for 2 h to ensure full acid-site coverage. Subsequently, the cell was evacuated for 30 min at 150 °C and 250 °C, and spectra were collected at each temperature. Particle-size distributions were determined in triplicate with a Malvern 2000 analyzer. CO_2-TPD was carried out on a Micromeritics Auto Chem II 2920 (USA). The sample was heated to 200 °C (10 °C/min, 30 min hold) in 30 mL/min He to remove moisture, cooled to 50 °C, saturated with 40 mL/min high-purity CO_2 for 60 min, and then purged with 30 mL/min He for 30 min to eliminate physisorbed CO_2. Desorption was monitored from 50 to 500 °C at 10 °C/min under 30 mL/min He.

2.3 Absorption and desorption experiments

CO_2 uptake and multi-cycle desorption experiments were conducted in a custom-designed semi-intermittent apparatus. During the absorption phase, a continuous stream of pure CO_2 (1.5 L /min) sequentially passed through a calibrated mass-flow meter, a three-way valve, and a wash bottle before entering into a 500 mL three-neck flask containing 30 wt.% MEA solution. The system was maintained at 40 ± 1 °C under constant magnetic stirring at 300 r/min [20,44]. To monitor the absorption progress, the solution of 1-1.5 mL was periodically withdrawn every 2-3 min using a pipette and collected in sealed vials for subsequent analysis. A bypass loop was integrated into the gas line to allow controlled interruption of CO_2 flow, which kept closed during absorption to maintain a stable gas supply, and was opened during sampling to divert the gas stream and temporarily suspend gas–liquid contact. This setup enabled the safe withdrawal of 1-2 mL of CO_2-loaded amine solution from the reactor headspace without disturbing the bulk system. After each sampling, the bypass valve was closed to restore CO_2 flow, and absorption continued until the MEA solution reached a CO_2 loading of 0.50 mol CO_2 per mole of amine, as measured by Chittick titration.

CO_2-desorption experiments were conducted in a 1 L three-neck flask fitted with a thermometer, condenser and sampling port. In each run, 2 g of catalyst was added to the CO_2-loaded MEA solution and the mixture was maintained at 90 ± 1 °C with magnetic stirring at 400 r/min [45,46]. The oil bath was insulated with black thermal cotton to minimize the heat loss and ensure an accurate temperature control. When the MEA temperature reached 40 °C, an initial aliquot of 1-1.5 mL was withdrawn for Chittick titration to determine the CO_2 loading. Subsequently, samples were collected

every 5 min initially, with intervals extended to 15 min between 30 and 60 min, and to 30 min between 60 and120 min. Electrical power consumption was recorded simultaneously by an energy meter. The CO_2 loading (α) was calculated from the volumes of CO_2 evolved and HCl consumed during the Chittick titration, as seen in Eq. (1):

$$\alpha=\frac{V_{CO2}-2V_{HCl}}{V_{HCl}\times\zeta} \quad (1)$$

Here, α denotes the CO_2 loading, V_{CO2} represents the volume of CO_2 evolved during the analysis, V_{HCl} corresponds to the volume of hydrochloric acid consumed at the titration endpoint (indicated by the complete colour change of the amine solution), and ζ is the gas-phase correction factor computed from $\zeta=\frac{(T+273.15)\times 22.4}{273.15}$.

For the catalytic desorption of CO_2 from MEA phase, the catalyst was compressed into a thin flake, encased in a fine-pore gauze, and positioned at the center of CO_2-rich MEA solution. Each experiment involved approximately twelve sampling steps, leading to a MEA volume reduction of 20-30 mL, which occupies 4-6% of the initial 500 mL. As reported in the literature, the CO_2 desorption rate is primarily determined by the MEA^+COO^- concentration in the loaded solution [47]. Consequently, this minor solvent loss does not alter amine concentration and is therefore considered kinetically negligible [48].

Herein, CO_2-desorption profiles were constructed by plotting the CO_2 loading (mol/mol) versus residence time (min) from the initial saturated value of 0.5 mol/mol to the equilibrium lean loading in the MEA solvent. Each loading datum was obtained in duplicate (or more) to guarantee an average absolute deviation (AAD) below 5%. The figures-of-merit used to appraise CO_2-desorption performance-namely, the molar amount of CO_2 released (n_{CO_2}), the mean desorption rate (r), the absolute heat duty (HD), the relative heat duty (RHD), the cyclic capacity and the composite desorption parameter (DP), are defined and computed in Eqs. (2-7), as detailed below:

$$n_{CO_2}=C\times V\times(\alpha_{rich}-\alpha_{lean}) \quad (2)$$

$$r=\frac{n_{CO_2}}{dt}=\frac{C\times V\times(\alpha_{rich}-\alpha_{lean})}{dt} \quad (3)$$

$$HD=\frac{Q_{input}}{n_{CO_2}}=\frac{kJ/h}{mol/h} \quad (4)$$

$$RHD=\frac{HD_i}{HD_{baseline}}\times 100\% \quad (5)$$

$$Cyclic\ capacity=C\times(\alpha_{rich}-\alpha_{lean}) \quad (6)$$

$$Desorption\ parameter = \frac{initial\ desorption\ rate \times cyclic\ capacity}{heat\ duty} \quad (7)$$

3.Results and discussion

3.1 Catalytic Desorption and Absorption Performance Evaluation

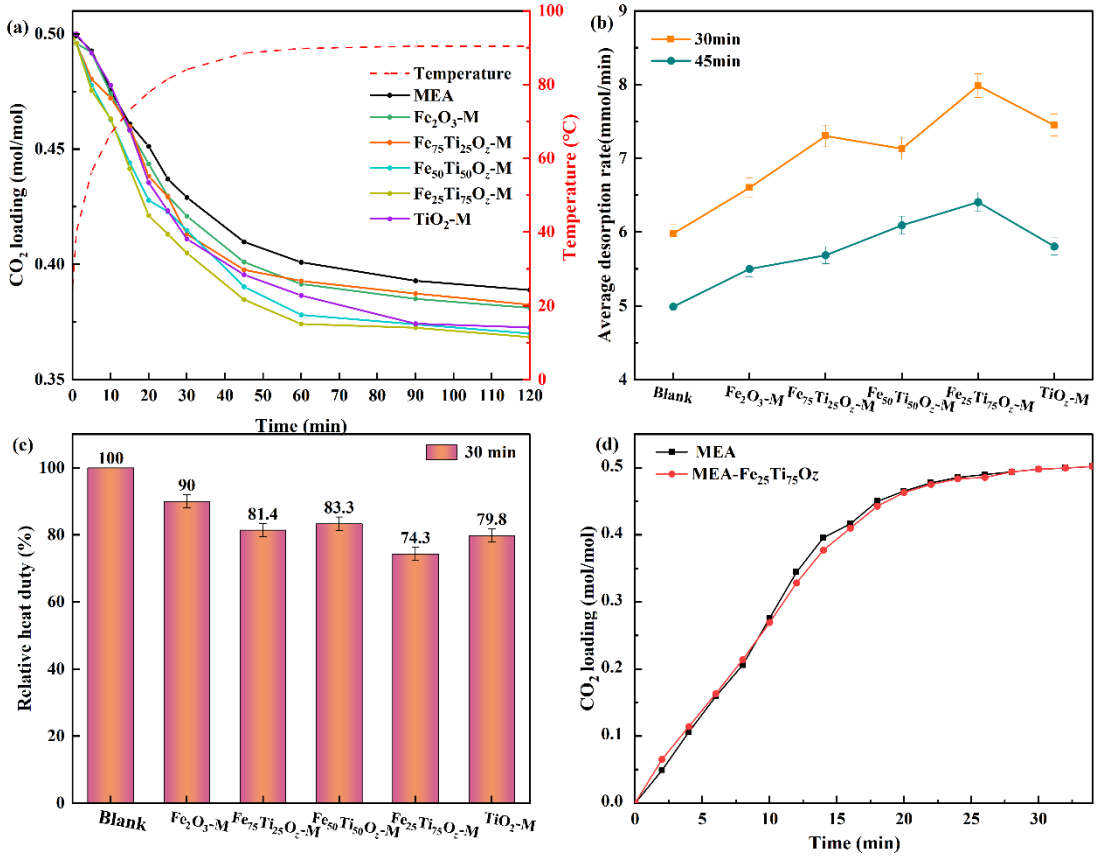

Fig.1. Catalytic desorption performance: CO_2 desorption profiles (a), average desorption rate (b), relative heat duty (c), and catalytic effect of $Fe_{25}Ti_{75}O_z$-M on CO_2 absorption (d).

The catalytic CO_2 desorption performance of the five as-synthesized catalysts was evaluated in 5 M MEA solution and benchmarked against a blank run (Fig. 1(a)). Between 40 ℃ and 90 ℃ all solids accelerated the reduction of CO_2 loading, the steepest decrease occurred within the first 30 min of the 120-min test, indicating an extremely rapid desorption rate. The rate declined progressively from 30-60 min and levelled off from 60-120 min. Consequently, the average desorption rate (ADR) over the initial 30 min and the relative heat duty were used as the main metrics of catalytic activity. As shown in Fig. 1(b), the 30-min ADR displays a volcano-type trend with increasing Fe/Ti molar ratio, peaking at Fe/Ti = 25/75, where the ADR is 36% higher than that of the uncatalyzed system. Correspondingly, the RHD values (Fig. 1(c)) indicate that $Fe_{25}Ti_{75}O_z$-M reduces energy consumption by 25.7%, ranking superior to TiO_2-M, $Fe_{75}Ti_{25}O_z$-M, $Fe_{50}Ti_{50}O_z$-M,

and Fe_2O_3-M. These results demonstrate that $Fe_{25}Ti_{75}O_z$-M not only accelerates CO_2 desorption but also substantially lowers the energy requirement for solvent regeneration, underscoring its potential for cost-effective and energy-efficient CO_2 capture. To verify whether the acidic solids impair absorption, absorption tests were conducted, as seen in Fig. 1(d). In 5 M MEA the catalysts slightly enhance the rate in the first 10 min, but the final CO_2 loading (0.50 ± 0.01 mol mol^{-1}) is identical to that without catalyst, confirming that the absorption equilibrium is unaffected. Table 1 summarizes the cyclic capacities and desorption parameters for the first 30 min. As the Fe content decreases, the cyclic capacity increases and the heat duty decrease. Among the tested catalysts, $Fe_{25}Ti_{75}O_z$-M exhibits the highest composite desorption parameter, with an RDF of 258.8% relative to the blank, highlighting its superior combination of desorption efficiency, energy savings, and operational stability for practical CO_2 capture applications.

Table 1. Desorbed amount, heat duty and desorption parameter of CO_2 within the first 30 min from MEA solution over the as-prepared catalysts.

Catalysts	Cyclic capacity (*10^3 mol CO_2)	Heat duty (kJ/mol)	Desorption parameter [(10^{-3} mol CO_2)^3/L^2 kJ mol]
Blank	0.176	1185.18	0.0017
TiO_2-M	0.223	934.4	0.0036
$Fe_{25}Ti_{75}O_z$-M	0.240	871.6	0.0044
$Fe_{50}Ti_{50}O_z$-M	0.214	975.9	0.0031
$Fe_{75}Ti_{25}O_z$-M	0.219	953	0.0034
Fe_2O_3-M	0.198	1054.4	0.0025

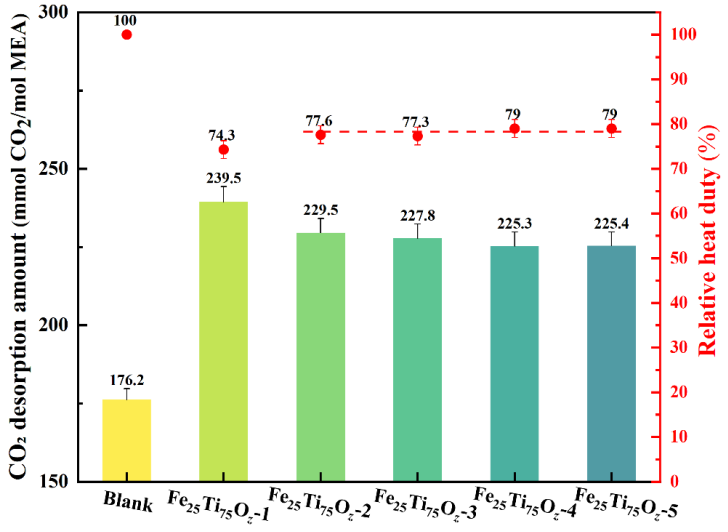

Fig. 2. Cyclic stability test of $Fe_{25}Ti_{75}O_z$-M catalyst: CO_2 desorption amount and relative heat duty over five consecutive regeneration cycles.

Catalyst stability is a key property for realizing catalyst recycling and cost reduction. The $Fe_{25}Ti_{75}O_z$-M catalyst was subjected to five consecutive CO_2 desorption cycles in an amine-rich solution at a catalyst-to-MEA mass ratio of 0.4 wt. %. After each cycle, the wrapped sheet-like catalyst was removed, repeatedly rinsed with deionized water to eliminate residual amine on the surface, dried, and then reused in the next cycle. As shown in Fig. 2, the fresh $Fe_{25}Ti_{75}O_z$-M catalyst achieved a CO_2 desorption amount of 239.5 mol over per mol MEA and a relative heat duty of 74.3 %. After five cycles, it retained approximately 95% of its initial desorption capacity, and the relative heat duty increased only slightly to 79%, indicating minimal loss in catalytic activity. The XRD and FT-IR patterns of the fresh and spent $Fe_{25}Ti_{75}O_z$-M catalysts are presented in Fig. 3. After five cycles, the spent catalyst retains an amorphous phase similar to that of the fresh sample, except for the emergence of weak TiO_2-M diffraction peaks, likely arising from interactions between Fe and Ti species during use. Compared with the fresh catalyst, the FT-IR spectrum of the spent $Fe_{25}Ti_{75}O_z$-M shows enhanced bands at 3420 cm^{-1} and 1630 cm^{-1}, attributed to surface-adsorbed water, along with a slightly intensified band at 1407 cm^{-1} corresponding to sulfated species [49]. Notably, a new signal at 1078 cm^{-1} in the spent catalyst is probably due to MEA adsorbed on the surface [50]. In addition, the diffraction peak around 500 cm^{-1} shifts slightly, indicating lattice inter-doping and strong mutual interactions, consistent with the XRD observations. Although the spent-catalyst exhibits minor structural rearrangement and adsorption of a small amount of MEA during cycling, it still retains 95% of original catalytic CO_2 desorption capacity with the relative heat duty increasing from 74.3% to 79% in the fifth test, indicating that the as-prepared $Fe_{25}Ti_{75}O_z$-M catalyst possesses a certain degree of stability, and its abundant hydroxyl groups and sulfate species may play a positive role in promoting carbamate decomposition. In addition, Table 2 presents a comparison of CO_2 desorption performance over various solid acid catalysts for CO_2-rich MEA amine solutions. From Table 2, it can be seen that the as-prepared $Fe_{25}Ti_{75}O_z$-M catalyst effectively increases the CO_2 desorption amount and reduces the consumption of renewable energy at 90 °C, which is better than most of the solid acid catalysts reported in Table 2.

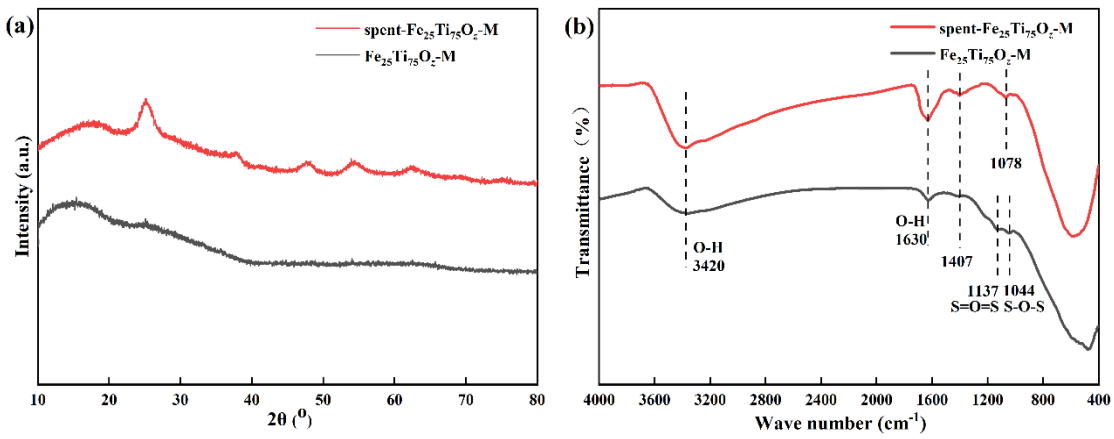

Fig.3. XRD patterns (a) and FT-IR spectra (b) of the fresh $Fe_{25}Ti_{75}O_z$-M and spent $Fe_{25}Ti_{75}O_z$-M catalysts.

Table 2 Comparison of catalytic activity over various solid acid catalysts for the regeneration of MEA solution

Catalysts	Catalyst loading (wt.%)	Desorption temperature (°C)	Increase in desorbed CO_2 (%)	Relative heat duty (%)	Ref.
NiO-KIT-6	1.25	100	-	75.4	[50]
SO_4^{2-}/TiO_2	1.5	96	20.0	82.9	[51]
SAPO-34	1.5	96	28.3	75.7	
SO_4^{2-}/ZrO_2	1.25	96	20	88.9	[52]
SO_4^{2-}/SnO_2	1.25	96	37.5	75.6	
TiO_2	0.42	90	-	89.7	
MOR	0.42	90	-	88.4	[53]
HZSM-5	0.42	90	-	84.1	
TiP_2O_7	0.1	91	14.2	87.0	
TiO_2	0.1	91	8.8	92.0	[54]
TiC	0.2	91	12.0	90.0	
Al_2O_3	1.25	96	-	79.1	[55]
$Fe_{25}Ti_{75}O_z$-M	0.4	90	36.0	74.3	This work

3.2 Catalyst Characterization Results

The $Fe_{25}Ti_{75}O_z$-M catalyst, identified as optimal in terms of Fe:Ti molar ratio, was subjected to detailed characterization, with TiO_2-M and Fe_2O_3-M serving as references. Fig. 4(a) shows the XRD patterns of TiO_2-M, Fe_2O_3-M and $Fe_{25}Ti_{75}O_z$-M. TiO_2-M and Fe_2O_3-M are both crystalline, matching the standard cards of anatase (JCPDS 21-1272) and hematite (JCPDS 99-0060), respectively. Compared with the sharp reflections of Fe_2O_3-M, the peaks of TiO_2-M are broader, indicating that sulfation suppresses crystal growth. In contrast, the diffraction profile of the bimetallic $Fe_{25}Ti_{75}O_z$-M catalyst is essentially amorphous. The similar saturation coordination numbers of Fe and Ti induce severe lattice distortion, preventing the formation of well-defined

crystalline phases [39]. Such amorphous structures typically provide high surface areas, large pore volumes, and abundant functional groups, all conducive to accelerated CO_2 desorption from MEA solutions [21].

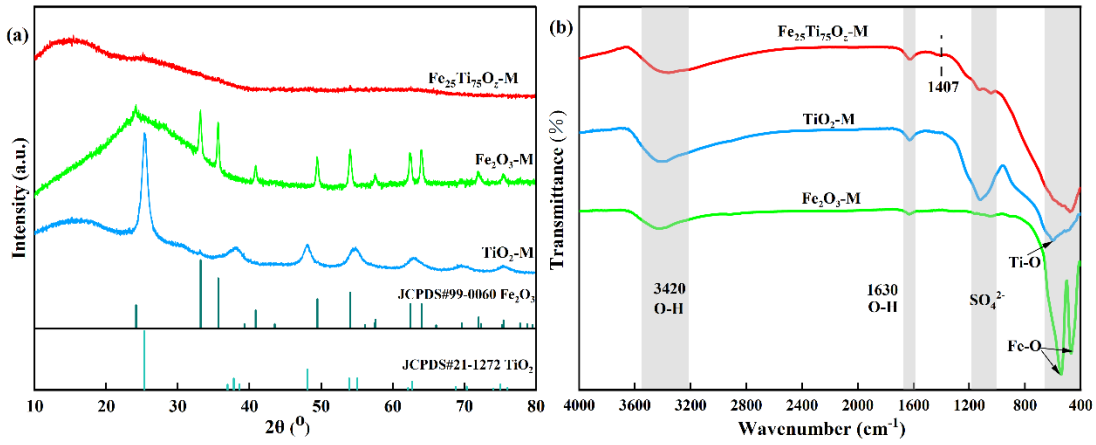

Fig.4. XRD patterns (a) and FT-IR spectra (b) of TiO_2-M, Fe_2O_3-M, and $Fe_{25}Ti_{75}O_z$-M catalysts.

The FT-IR spectra in Fig. 4(b) reveals bands at 3420 cm^{-1} and 1630 cm^{-1} assigned to the stretching and bending vibrations of surface-adsorbed H_2O (-OH). The feature near 500 cm^{-1} corresponds to Fe-O and Ti-O stretching. Absorptions between 900 cm^{-1} and 1300 cm^{-1} are associated with S-O stretching in inorganic chelates. For $Fe_{25}Ti_{75}O_z$-M, peaks at 1137 cm^{-1} and 1044 cm^{-1} are ascribed to O=S=O and O-S-O moieties, evidencing both bidentate bridging and chelating sulfate species [39,56]. Sulfate groups are strongly electron-withdrawing, and they extract electron density from adjacent Fe^{3+} and Ti^{4+} and simultaneously weaken surface -OH groups, thereby generating abundant Lewis-acid sites and proton-donating -OH groups [39,56]. Additionally, the band at 1407 cm^{-1} indicates two types of sulfated species on $Fe_{25}Ti_{75}O_z$-M, which are strongly electron-withdrawing, generating abundant Lewis acid sites and proton-donating -OH groups that facilitate carbamate decomposition, thereby lowering the energy requirement for amine regeneration [39,57].

X-ray photoelectron spectroscopy (XPS) was used to verify the surface chemistry and elemental states of TiO_2-M and $Fe_{25}Ti_{75}O_z$-M. As shown in Fig. 5, Ti, Fe, S and O are detected on $Fe_{25}Ti_{75}O_z$-M, confirming successful synthesis. Peaks at 464.6 eV (Ti $2p_{1/2}$) and 458.8 eV (Ti $2p_{3/2}$) are assigned to Ti-O-S and Ti-O bonds, respectively, evidencing surface Ti^{4+} [39,56]. S $2p_{1/2}$ (169.8 eV) and S $2p_{3/2}$ (178.7 eV) signals correspond to S^{6+}, indicating sulfate incorporation [39]. The O 1 s peaks at ~530.1 eV and ~530.8 eV are associated with lattice oxygen and lattice hydroxyls, whereas the component near 532 eV reflects oxygen in sulfate bonded to metal atoms [58]. After Fe

introduction, the binding energies shift to higher values, implying decreased electron density, likely due to Fe-Ti interactions. Importantly, Fe incorporation enriches the surface -OH population, which is crucial for carbamate decomposition. Finally, the Fe 2p envelope can be deconvoluted into eight sub-peaks: the component at 711.3 eV is assigned to Fe^{2+} $2p_{3/2}$ and that at 713.2 eV to Fe^{3+} $2p_{3/2}$. During operation, reversible redox cycling between Fe^{2+} and Fe^{3+} not only ensures catalyst recyclability but also generates abundant oxygen vacancies that enhance catalytic activity [27].

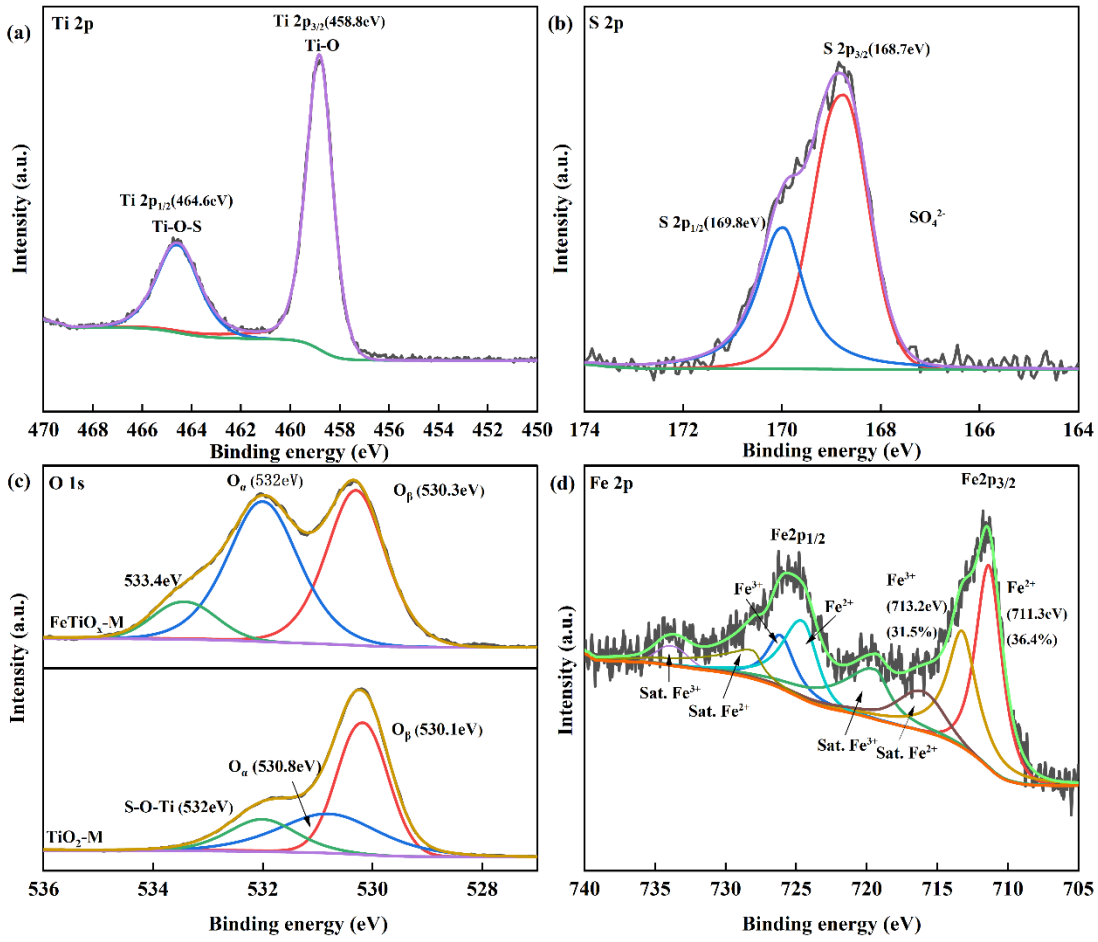

Fig.5. XPS spectra of TiO_2-M and $Fe_{25}Ti_{75}O_z$-M catalysts: (a) Ti 2p, (b) S 2p, (c) O 1s, and (d) Fe 2p.

The surface acidity of TiO_2-M, Fe_2O_3-M and $Fe_{25}Ti_{75}O_z$-M was quantified by NH_3 temperature-programmed desorption (NH_3-TPD). Desorption temperatures in the ranges 50-400 °C, 400-600 °C and > 600 °C are assigned to weak, medium and strong acid sites, respectively [39]. As shown in Fig. 6(a), Fe_2O_3-M exhibits negligible acidity, whereas TiO_2-M displays a pronounced desorption peak above 600 °C, indicating a high density of strong acid sites, which is consistent with XPS analysis. After Fe is incorporated into the Ti matrix, distinct desorption signals appear in all three temperature windows, indicating that Fe introduction not only preserves the strong sites

but also generates additional weak and medium-strength acid sites. This enrichment is attributed to the electron-withdrawing effect of sulfate on Lewis-acid centers. The type and abundance of acid sites are critical for carbamate decomposition. Py-IR spectra of TiO_2-M and $Fe_{25}Ti_{75}O_z$-M are compared in Fig. 6(b). Bands at 1446, 1576 and 1608 cm^{-1} are diagnostic of Lewis (L) acid sites, while those at 1488 cm^{-1} (L + B) and 1543 cm^{-1} (Brønsted, B) reflect combined Lewis/Brønsted and pure Brønsted acidity, respectively [49]. Both catalysts contain abundant L and B sites, however, quantitative analysis of Py-IR spectra at 150 and 250 °C (Table 3) shows that Fe doping largely preserves Brønsted acidity while significantly increasing Lewis acidity. This increase in Lewis sites enhances carbamate decomposition, corroborating the catalytic performance trends as aforementioned. Therefore, the cooperative interaction of Brønsted and Lewis acid sites is the key to the superior CO_2-desorption activity of $Fe_{25}Ti_{75}O_z$-M.

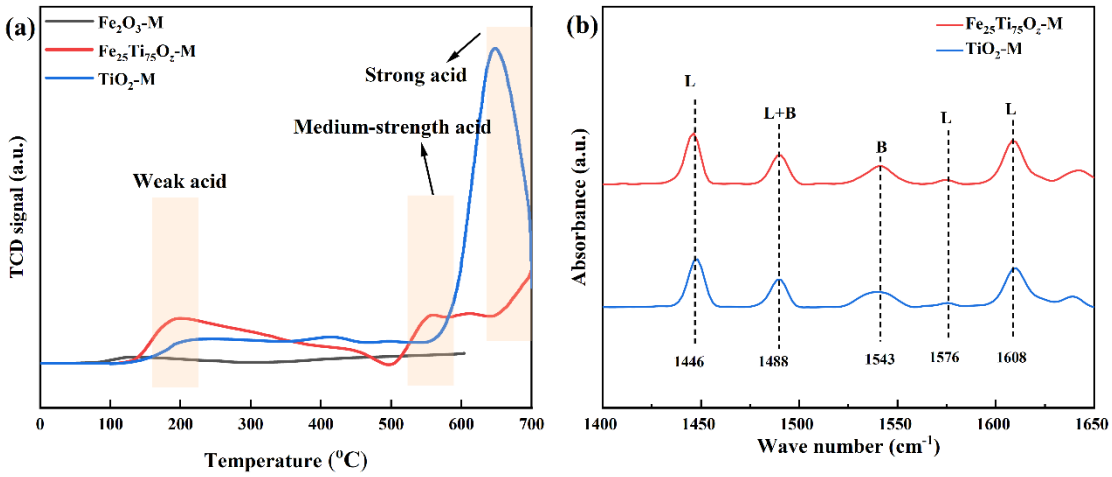

Fig.6. (a) NH_3-TPD profiles of TiO_2-M, Fe_2O_3-M, and $Fe_{25}Ti_{75}O_z$-M catalysts, (b) Py-IR spectra of TiO_2-M and $Fe_{25}Ti_{75}O_z$-M catalysts.

Table 3. Concentration and distribution of Lewis (L) and Brønsted (B) acid sites on TiO_2-M and $Fe_{25}Ti_{75}O_z$-M catalysts.

Samples	Weak acid (mmol/g)				Medium-strength acid (mmol/g)			
	B	L	B/L	Total	B	L	B/L	Total
TiO_2-M	0.061	0.077	0.78	0.138	0.04	0.051	0.84	0.089
$Fe_{25}Ti_{75}O_z$-M	0.063	0.082	0.76	0.145	0.04	0.048	0.79	0.079

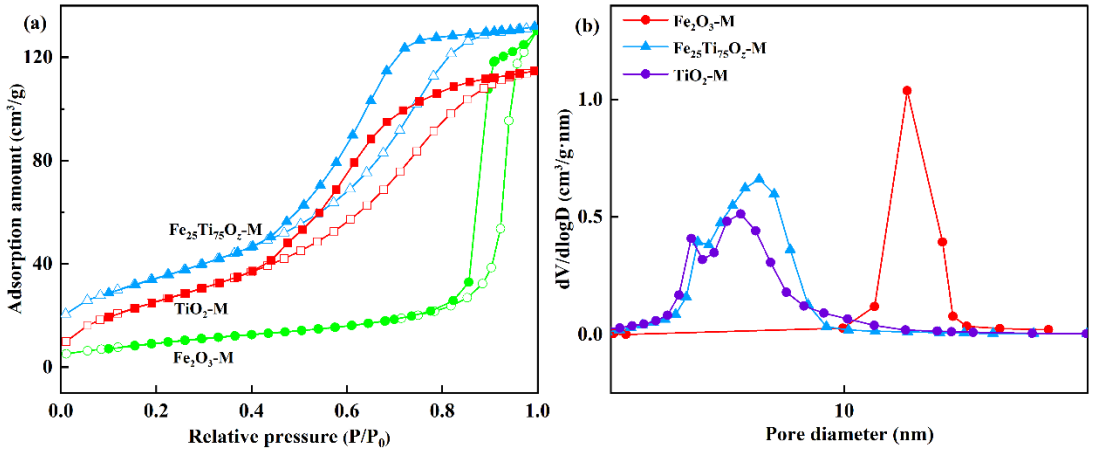

Fig.7. N_2 adsorption-desorption isotherms and corresponding pore-size distributions of TiO_2-M, Fe_2O_3-M and $Fe_{25}Ti_{75}O_z$-M catalysts

Fig. 7 presents the N_2 adsorption-desorption isotherms and corresponding pore-size distributions of TiO_2-M, Fe_2O_3-M and $Fe_{25}Ti_{75}O_z$-M catalysts. According to IUPAC classification, all three isotherms are type IV with well-defined H1 hysteresis loops in the relative pressure range 0.4-1.0, evidencing uniform micro-/mesoporous architectures [21,59]. Compared with Fe_2O_3-M, the low-pressure closure points of TiO_2-M and $Fe_{25}Ti_{75}O_z$-M shift to lower P/P_0 values. The approximate superimposable isotherms of $Fe_{25}Ti_{75}O_z$-M and TiO_2-M confirm intensive Fe-Ti lattice intermixing, consistent with XRD and IR results. Textural parameters are summarized in Table 4. $Fe_{25}Ti_{75}O_z$-M exhibits a slightly larger average pore diameter than TiO_2-M, yet smaller than Fe_2O_3-M, suggesting that Fe incorporation expands the Ti matrix pores and facilitates the carbamate diffusion into the catalyst interior. The mesoporous surface areas follow the order $Fe_{25}Ti_{75}O_z$-M > TiO_2-M > Fe_2O_3-M, with $Fe_{25}Ti_{75}O_z$-M displaying the highest BET area (125.6 m^2 g^{-1}). This increase in surface area and pore volume provides more exposed active sites and greater adsorption capacity for carbamate species, directly enhancing CO_2 desorption and accelerating amine regeneration.

Table 4. Physical structural parameters of TiO_2-M, Fe_2O_3-M and $Fe_{25}Ti_{75}O_z$-M catalysts.

Catalysts	BET surface area [a] (m^2/g)	Pore volume [b] (cm^3/g)	Pore diameter [c] (nm)
Fe_2O_3-M	36.1	0.19	16.3
TiO_2-M	100.6	0.17	4.5
$Fe_{25}Ti_{75}O_z$-M	125.6	0.21	4.7

a BET specific surface area

b BJH desorption pore volume

c BJH desorption pore diameter

3.3 Structure-Activity Relationship

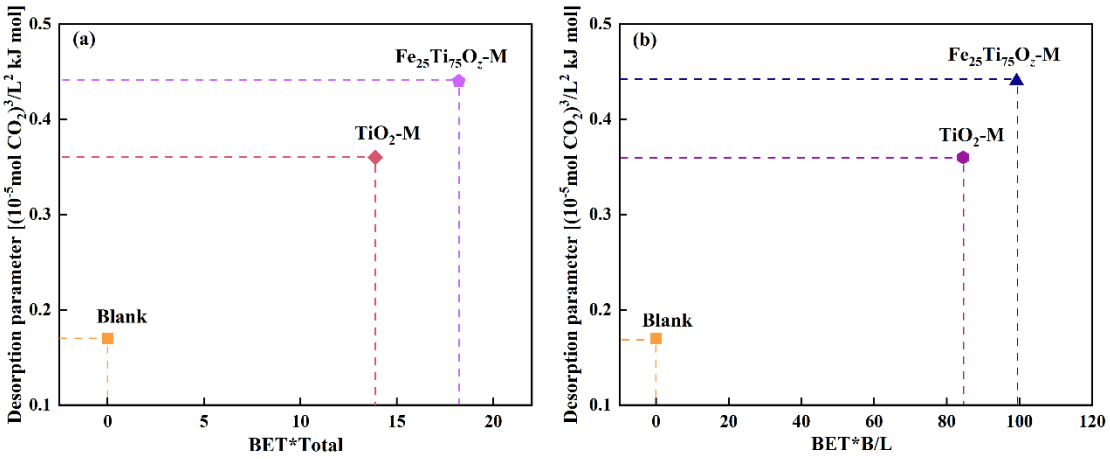

Fig.8. Influence of catalyst properties on CO_2 desorption performance: BET*Total (a) and BET*B/L (b).

As discussed above, the $Fe_{25}Ti_{75}O_z$-M catalyst exhibits superior CO_2 desorption performance compared with TiO_2-M due to its combination of a high BET surface area and abundant weak-acid sites, even though TiO_2-M possesses a greater total number of medium-strength acid sites and a larger Brønsted-to-Lewis (B/L) ratio. This indicates that the overall desorption efficiency arises from the cooperative interplay of multiple physicochemical factors including the total acidity, the Brønsted (B) sites, Lewis (L) sites, the B/L ratio, and the specific surface area. Fig. 8 illustrates the correlations between these properties and CO_2 desorption performance. Within it, Fig. 8(a) reveals a clear positive correlation between the desorption parameter and the BET × Total-acidity product, demonstrating that surface area and total acidity act synergistically to accelerate CO_2 release. A larger surface not only accommodates more acid sites but also increases the collision frequency with carbamate species, thereby raising the reaction rate. More interestingly, Fig. 8(b) shows an equally pronounced positive correlation between the desorption parameter and BET×B/L, with a sharp increase from TiO_2-M to $Fe_{25}Ti_{75}O_z$-M, emphasizing the critical role of Brønsted acidity in carbamate decomposition. It is explained that Brønsted sites directly donate protons to carbamate molecules, lowering the activation energy and reducing the heat requirement for amine regeneration.

4.Conclusions

In this study, a novel $FeTiO_z$-M composite catalyst was successfully developed via a microwave-assisted co-precipitation method, and the Fe:Ti molar ratio was systematically optimized to enhance CO_2 catalytic desorption from CO_2-rich MEA solutions. The results demonstrated that rational design of bimetallic solid-acid catalysts substantially improved both the

kinetics and energy efficiency of amine regeneration. At the optimized Fe:Ti ratio of 25:75, the loading of 0.4 wt. % catalyst resulted in the average CO_2 desorption rate increase by 36 % and the relative heat duty decreased by 25.7 %, thereby yielding a relative desorption parameter of 258.8 % with stable performance maintained over five cycles. Therefore, the catalyst not only significantly accelerated CO_2 desorption while reducing regeneration energy, but also exhibited certain cyclic stability over multiple absorption-desorption cycles, and this result laid a foundation for subsequent long-term continuous operation tests to explore its practical application feasibility. Mechanistic investigations revealed that the superior performance arisen from the synergistic interplay of structural and chemical properties, and the formation of an amorphous Fe-Ti solid solution increased mesoporous surface area and pore volume, facilitating carbamate diffusion. Furthermore, the introduction of sulfate groups activated surface hydroxyls and metal acid sites, providing abundant protons for carbamate decomposition, and the balanced distribution of Brønsted and Lewis acid sites ensured efficient CO_2 liberation with minimal energy input. These findings underscore the critical role of tailored surface chemistry and hierarchical porosity in optimizing catalytic performance.

CRediT authorship contribution statement

Mengyao Wang: Writing - original draft, Methodology, Validation. **Yanping Du, Haoran Zhang and Junge Lv:** Validation and Methodology. **Huancong Shi, Wei Lu and Jing Jin:** Investigation, Supervision, Writing - review & editing, Funding acquisition. **Zhibo Xiong:** Conceptualization, Funding acquisition, Writing - review & editing.

Declaration of Competing Interest

The authors declare that they have no known competing financial interests or personal relationships that could have appeared to influence the work reported in this paper.

Acknowledgements

This work was supported by the National Science Foundation of China (No. 51406118), the Bureau of Shanghai Municipal Science and Technology (No. 23010503500) and General program of Shanghai Natural Science Foundation (No. 21ZR1461900).

References

[1] Zhihan Fan, Qianlin Zhu, Yonggang Jia. Characteristics and monitoring plan in the atmosphere of CO_2 leakage

404 from carbon capture and storage projects. Environment, Development and Sustainability, 27(2025) 10399-
405 10414. https://doi.org/10.1007/s10668-023-04315-5.
406 [2] Friday O. Ochedi, Dongjing Liu, Jianglong Yu, Arshad Hussain, Yangxian Liu. Photocatalytic, electrocatalytic
407 and photoelectrocatalytic conversion of carbon dioxide: a review. Environmental Chemistry Letters,
408 19(2021)941-967. https://doi.org/10.1007/s10311-020-01131-5.
409 [3] Enobong Hanson, Chukwuebuka Nwakile, Victor Oluwafolajimi Hamme. Carbon capture, utilization, and
410 storage (CCUS) technologies: Evaluating the effectiveness of advanced CCUS solutions for reducing CO_2
411 emissions. Results in Surfaces and Interfaces, 18(2025)100381. https://doi.org/10.1016/j.rsurfi.2024.100381.
412 [4] Yafei Guo, Chang Tan, Jian Sun, Weiling Li, Jubing Zhang, Chuanwen Zhao. Biomass ash stabilized MgO
413 adsorbents for CO_2 capture application. Fuel, 259(2020) 116298. https://doi.org/10.1016/j.fuel.2019.116298.
414 [5] Xinxin Liu, Hui Zhang, Jie Du, Jianhe Liao. Research progress of methanol production via CO_2 hydrogenation:
415 Mechanism and catalysts. Process Safety and Environmental Protection, 189((2024)1071-1086.
416 https://doi.org/10.1016/j.psep.2024.07.018.
417 [6] Virginia Signorini, Anu Muthukamatchi, Luca Ansaloni, Thijs A. Peters, Ben Alcock, Maurizio Fiorini, Marco
418 Giacinti Baschetti, and Matteo Minelli. Physical, Mechanical, and Thermal Characterization of the Elastomer
419 Response to High-Pressure CO_2 for Use in Carbon Capture and Storage Applications. Industrial & Engineering
420 Chemistry Research, 64(2025)6704-6716. https://doi.org/10.1021/acs.iecr.4c04452.
421 [7] Jieping Han, Jiachun Li, Xi Tang, Lechen Wang, Xiaolong Yang, Zeqi Ge, Fei Yuan. Coal-fired power plant
422 CCUS project comprehensive benefit evaluation and forecasting model study. Journal of Cleaner Production,
423 385 (2023) 135657. https://doi.org/10.1016/j.jclepro.2022.135657.
424 [8] Xiaowen Yu, Hao Wu, Wenrui Li and Hongmin Yang. Emission characteristics of ethanolamine and ammonia in
425 CO_2 capture process by chemical absorption based on ethanolamine solution. Journal of Chemical Technology
426 & Biotechnology, 100 (2025) 688-696. https://doi.org/10.1002/jctb.7809.
427 [9] Jose Antonio Garci, Maria Villen-Guzman, Jose Miguel Rodriguez-Maroto, Juan Manuel Paz-Garcia. Technical
428 analysis of CO_2 capture pathways and technologies. Journal of Environmental Chemical Engineering, 10 (2022)
429 108470.https://doi.org/10.1016/j.jece.2022.108470.
430 [10] Friday O. Ochedi, Jianglong Yu, Hai Yu, Yangxian Liu, Arshad Hussain. Carbon dioxide capture using liquid
431 absorption methods: a review. Environmental Chemistry Letters, 19 (2021) 77-109.
432 https://doi.org/10.1007/s10311-020-01093-8.
433 [11] Hangqi Yan, Xueyan Hou, Lijian Ji, Hang Y, Wenrui Li, Sining Kon, Shudan Chi, Xin Wang, Dawei Hou, Linjun

Yang. Energy-efficient CO_2 capture using novel low-viscosity water-lean aromatic amine solvent MBA/BDMA/EG/H_2O: Performance, mechanism and thermodynamics. Separation and Purification Technology, 359 (2025) 130391. https://doi.org/10.1016/j.seppur.2024.130391.

[12] Lijian Jin, Xueyan Hou, Lingxiao Zhan, Shangzhi Xie, Lina Gu, Hangqi Yang, Xin Wang, Xinfeng Qian, Jianchong Shen, Linjun Yang. Capturing CO_2 using novel nonaqueous biphasic solvent TMEDA/MEA/DMSO: Absorption and phase splitting mechanism. Chemical Engineering Journal, 484 (2024) 149293. https://doi.org/10.1016/j.cej.2024.149293.

[13] Guangjie Chen, Guangying Chen, Miao Fa, Yuxian Yang, Yu Wang, Fei Li, LiSze Lai, SweePin Yeap. Potential of a-Amino-2-Propanol/Sulfolane Biphasic Solution for CO_2 Capture: Performance and Mechanism Study. Energy Fuels 38 (2024) 17726-17740. https://doi.org/10.1021/acs.energyfuels.4c02734.

[14] Guangjie Chen, Guangying Chen, Liuyi Yin, Fei Li, Li Sze Lai, Wee Horng Tay, Swee Pin Yeap, Lin Jin. Performance and mechanism investigation of CO_2 capture by novel ternary MEA/tertiary amine/sulfolane biphasic solvents. International Journal of Greenhouse Gas Control 146 (2025) 104436. https://doi.org/10.1016/j.ijggc.2025.104436.

[15] Guangjie Chen, Guangying Chen, Maurizio Peruzzini, Francesco Barzagli, Rui Zhang. Investigating the Performance of Ethanolamine and Benzylamine Blends as Promising Sorbents for Post combustion CO_2 Capture through ^{13}C NMR Speciation and Heat of CO_2 Absorption Analysis. Energy Fuels. 36 (2022) 9203−9212. https://doi.org/10.1021/acs.energyfuels.2c01930.

[16] Hope McLaughlin, Anna A. Littlefield, Maia Menefee, Austin Kinzer, Tobias Hull, Benjamin K. Sovacool, Morgan D. Bazilian, Jinsoo Kim, Steven Griffiths. Carbon capture utilization and storage in review: Sociotechnical implications for a carbon reliant world. Renewable and Sustainable Energy Reviews, 177 (2023) 113215. https://doi.org/10.1016/j.rser.2023.113215.

[17] Fanzhi Meng, Yuan Meng, Tongyao Ju, Siyu Han, Li Lin, Jianguo Jiang. Research progress of aqueous amine solution for CO_2 capture: A review. Renewable and Sustainable Energy Reviews, 168 (2022) 112902. https://doi.org/10.1016/j.rser.2022.112902.

[18] Sunkyung Kim, Hu Shi, Jin Yong Lee. CO_2 absorption mechanism in amine solvents and enhancement of CO_2 capture capability in blended amine solvent. International Journal of Greenhouse Gas Control, 45 (2016) 181-188. http://dx.doi.org/10.1016/j.ijggc.2015.12.024.

[19] Jessica Narku-Tetteh, Pailin Muchan, Chintana Saiwan, Teeradet Supap, Raphael Idem. Selection of components for formulation of amine blends for post combustion CO_2 capture based on the side chain structure

of primary, secondary and tertiary amines. Chemical Engineering Science, 170 (2017) 542-560. http://dx.doi.org/10.1016/j.ces.2017.02.036.

[20] Yunzhao Guo, Huiping Zhang, Kaiyun Fu, Xianfu Chen, Minghui Qiu, Yiqun Fan. Integration of solid acid catalyst and ceramic membrane to boost amine-based CO_2 desorption. Energy, 274 (2023) 127329. https://doi.org/10.1016/j.energy.2023.127329.

[21] Haoran Zhang, Junge Lv, Zhibo Xiong, Huancong Shi, Jing Jin, Mengqi Liu, Yanping Du, Wei Lu. Promotional effect of microwave radiation treatment on the desorption of CO_2 from mono-ethanolamine (MEA) solution over FeOOH catalyst. Journal of Environmental Chemical Engineering, 12 (2024) 114382. https://doi.org/10.1016/j.jece.2024.114382.

[22] Lidong Wang, Aizimaitijiang Aierken, Lei Xing, Qin Dai, and Guangfei Yu. Applied Machine Learning for Prediction of Energy-Efficient CO_2 Desorption on Solid Acid Catalysts. Environmental Science & Technology, 59(2025) 16490-16500. https://doi.org/10.1021/acs.est.5c01841.

[23] Yingjie Niu, Shiying Zou, Haonan Liu, Minyue Hu, Jinjun Cai, Chao'en Li, Kathryn A. Mumford, Masood S. Alivand, Francesco Barzagli, Rui Zhang. Functionalized SBA-15-based catalysts for energy-efficient CO_2 desorption: Bridging experimentation and machine learning to enhance amine sorbents regeneration. Chemical Engineering Journal, 522 (2025) 167944. https://doi.org/10.1016/j.cej.2025.167944

[24] Xiaowen Zhang, Cong Xiang, Shijian Lu, Zhan Tan, Yushan Kai, Jiayu Mao, Yansong Yang, Fangfang Zhao, Kuiyi You, He'an Luo. Synergistic enhancement of CO_2 desorption by a novel MEA-EAE-3DEA1Ptri-solvent: comparative study with solid acid catalysts. Chemical Engineering Journal, 523 (2025) 168647. https://doi.org/10.1016/j.cej.2025.168647.

[25] Kexin Wei, Lei Xing, Yuchen Li, Teng Xu, Qiangwei Li, Lidong Wang. Heteropolyacid modified cerium-based MOFs catalyst for amine solution regeneration in CO_2 capture. Separation and Purification Technology, 2022, 293:121144. https://doi.org/10.1016/j.seppur.2022.121144.

[26] Minhua Li, Saeed Askari, Yingjie Niu, Ting Li, Ali Zavabeti, Masood S. Alivand, Kathryn A. Mumford, Chao' en Li, Rui Zhang. One-step synthesis of SO_4^{2-}/ZrO_2-SEP solid-acid catalyst for energy-efficient CO_2 capture. Separation and Purification Technology, 359 (2025) 130577. https://doi.org/10.1016/j.seppur.2024.130577.

[27] Li Rao, Bangheng Jin, Dong Chen, Xin Jin, Guangrong Liu, Zilin Huang, Kaihong Cao, Fangyue Chen, Qiang Huang. Energy-saving CO_2 desorption from amine solution over Fe/SiO_2/biochar catalysts: desorption performance, structure-activity relationship, and mechanism. Chemical Engineering Journal, 483 (2024) 149413. https://doi.org/10.1016/j.cej.2024.149413.

[28] Xin Jin, Xinyu Zhao, Bangheng Jin, Long Tong, Zekun Xu, Mingrui Cao, Guangrong Liu, Jinli Zhai, Zhihe Yang, Qiang Huang. Integrated solid acid catalysis and photothermal conversion to regenerate CO_2-captured amine solutions using black TiO_2 nanoparticles. Chemical Engineering Journal, 522 (2025) 167295. https://doi.org/10.1016/j.cej.2025.167295.

[29] Yihang Zhou, Yijiang Tian, Min Shi, Zhen Tian, Yibo Zhou, Yuan Zhang, Wenzhong Gao. How TiO_2, SiO_2, and ZnO nanofluids differentially enhance CO_2 absorption-desorption in MEA through heat and mass transfer mechanisms. Applied Thermal Engineering, 278 (2025) 127463. https://doi.org/10.1016/j.applthermaleng.2025.127463.

[30] Ahmed M. Abudeeb, Mahmoud N. Almakhadmeh, Sagheer A. Onaizi. CO_2 Capture using functionalized metal organic frameworks: A review. Surfaces and Interfaces, 72 (2025) 107381. https://doi.org/10.1016/j.surfin.2025.107381.

[31] The Ky Vo, Woo-Sik Kim, and Jinsoo Kim. Ethylenediamine-incorporated MIL-101(Cr)-NH_2 metal-organic frameworks for enhanced CO_2 adsorption. Korean Journal of Chemical Engineering, 37(2020) 1206-1211. https://doi.org/10.1007/s11814-020-0548-8.

[32] Zhan Tan, Xiaowen Zhang, Shangshang Zhang, Yi Peng, Sisi Zhao, Cong Xiang, Xinwei Yue, Fangfang Zhao, Kuiyi You, He'an Luo. Enhancing CO_2 desorption rate in rich MEA solutions by metal-modified attapulgite catalyst. Separation and Purification Technology, 330 (2024) 125513. https://doi.org/10.1016/j.seppur.2023.125513.

[33] Masood S. Alivand, Omid Mazaheri, Yue Wu, Geoffrey W. Stevens, Colin A. Scholes, and Kathryn A. Mumford. Catalytic Solvent Regeneration for Energy-Efficient CO_2 Capture. ACS Sustainable Chemistry & Engineering, 8 (2020) 18755-18788.https://doi.org/10.1021/acssuschemeng.0c07066.

[34] Umair H. Bhatti, Sungchan Nam, Sungyoul Park and Il Hyun Baek. Performance and Mechanism of Metal Oxide Catalyst-Aided Amine Solvent Regeneration. ACS Sustainable Chemistry & Engineering, 6 (2018) 12079-12087. https://doi.org/10.1021/acssuschemeng.8b02422.

[35] Lei Xing, Kexin Wei, Yuchen Li, Zhimo Fang, Qiangwei Li, Tieyue Qi, Shanlong An, Shihan Zhang, and Lidong Wang. TiO_2 Coating Strategy for Robust Catalysis of the Metal-Organic Framework toward Energy-Efficient CO_2 Capture. Environmental Science & Technology, 55 (2021) 11216-11224. https://doi.org/10.1021/acs.est.1c02452.

[36] Yuchen Li, Zhen Chen, Guoxiong Zhan, Bingling Yuan, Lidong Wang, Junhua Li. Inducing efficient proton transfer through Fe/Ni@COF to promoteamine-based solvent regeneration for achieving low-cost capture of

CO_2 from industrial flue gas. Separation and Purification Technology, 298 (2022) 121676. https://doi.org/10.1016/j.seppur.2022.121676.

[37] Ankit Mishra, Vikas Verma, Azeem Khan, Dileep Kumar, Tuhin Suvra Khan, Vipin Amoli, Anil Kumar Sinha. Waste ilmenite sludge-derived low-cost mesoporous Fe-doped TiO_2: A versatile photocatalyst for enhanced visible light photocatalysis without a cocatalyst. Journal of Environmental Chemical Engineering, 11 (2023) 110319. https://doi.org/10.1016/j.jece.2023.110319.

[38] Jiazong Jiang, Bo Zhao, Yuqun Zhuo, Shujuan Wang. Experimental study of CO_2 absorption in aqueous MEA and MDEA solutions enhanced by nanoparticles. International Journal of Greenhouse Gas Control, 29 (2014) 135-141. http://dx.doi.org/10.1016/j.ijggc.2014.08.004.

[39] Zanbu Geng, Yang Yang, Yixi Wang, Tingyu Zhu, Wenqing Xu. Catalytic regeneration of amine-based absorbents for CO_2 capture: The effect of acidic sites and accessibility. Separation and Purification Technology, 327 (2023) 124889. https://doi.org/10.1016/j.seppur.2023.124889.

[40] Xiong Zhibo, Wu Chao, Hu Qiang, Wang Yongzhen, Jin Jing, Lu Chunmei, Guo Dongxu. Promotional effect of microwave hydrothermal treatment on the low-temperature NH_3-SCR activity over iron-based catalyst. Chemical Engineering Journal, 286 (2016) 459-466. http://dx.doi.org/10.1016/j.cej.2015.10.082.

[41] Ding Chen, Yingzhe Zhang. Synthesis of $NiFe_2O_4$ nanoparticles by a low temperature microwave-assisted ball milling technique. Science China Technological Sciences, 55(2012)1535-1538. https://doi.org/10.1007/s11431-012-4772-2.

[42] Mustafa Erguvan, Shahriar Amini. Experimental microwave assisted CO_2 desorption of a solid sorbent in a fluidized bed reactor. Separation and Purification Technology, 343 (2024) 127062. https://doi.org/10.1016/j.seppur.2024.127062.

[43] Fangui Nie, Hongyang Sun, Xiaonan Liu, Jicheng Zhou, Wentao Xu. Enhanced microwave-catalytic performance for CO_2 oxidative propane dehydrogenation by acidified and Bi-doped ZnO-based microwave catalysts. Journal of Environmental Chemical Engineering, 12 (2024) 114291. https://doi.org/10.1016/j.jece.2024.114291.

[44] Umair H. Bhatti, Abdul K. Shah, Jeong Nam Kim, Jong Kyun You, Soo Hyun Choi, Dae Ho Lim, Sungchan Nam, Yeung Ho Park, and Il Hyun Baek. Effects of Transition Metal Oxide Catalysts on MEA Solvent Regeneration for the Post-Combustion Carbon Capture Process. ACS Sustainable Chemistry & Engineering, 5 (2017) 5862-5868. https://doi.org/10.1021/acssuschemeng.7b00604.

[45] Masood S. Alivand, OmidMazaheri, YueWu, Geoffrey W. Stevens, Colin A. Scholes and Kathryn A. Mumford.

554 Catalytic Solvent Regeneration for Energy -Efficient CO_2 Capture. ACS Sustainable Chemistry & Engineering,
555 8 (2020) 18755-18788. https://dx.doi.org/10.1021/acssuschemeng.0c07066.
556 [46] Cong Jiang, Maohong Fan, Ge Gaob, Wufeng Jiang, Xiaoshan Li, Cong Luo, Liqi Zhang, Fan Wu.
557 Nanostructured AlOOH---A promising catalyst to reduce energy consumption for amine-based CO_2 capture.
558 Separation and Purification Technology, 303 (2022) 122232. https://doi.org/10.1016/j.seppur.2022.122232.
559 [47] Huancong Shi, Junxing Fu, Qiming Wu, Min Huang, Linhua Jiang, Mingqi Cui, Raphael Idem, Paitoon
560 Tontiwachwuthikul. Studies of the coordination effect of DEA-MEA blended amines (within 1+4 to 2+3M)
561 under heterogeneous catalysis by means of absorption and desorption parameters. Separation and Purification
562 Technology, 236 (2020) 116179. https://doi.org/10.1016/j.seppur.2019.116179.
563 [48] Umair H. Bhatti, Dharmalingam Sivanesan, Dae Ho Lim, Sung Chan Nam, Sungyoul Park, Il Hyun Baek. Metal
564 oxide catalyst-aided solvent regeneration: A promising method to economize post-combustion CO_2 capture
565 process. Journal of the Taiwan Institute of Chemical Engineers, 93 (2018) 150-157.
566 https://doi.org/10.1016/j.jtice.2018.05.029.
567 [49] Xitong Yang, Ruifeng Zhou, Guowei Liu, Sajjad Hussain, Qiuye Li. Reduce energy consumption for organic
568 amine regeneration by MnOOH/HZSM-5 catalysts. Chemical Engineering Journal, 493 (2024) 152564.
569 https://doi.org/10.1016/j.cej.2024.152564.
570 [50] Rui Zhang, Ting Li, Yiming Zhang, Junyu Ha, Yuting Xiao, Chao'en Li, Xiaowen Zhang, He'an Luo. CuO
571 modified KIT-6 as a high-efficiency catalyst for energy-efficient amine solvent regeneration. Separation and
572 Purification Technology, 300 (2022) 121702. https://doi.org/10.1016/j.seppur.2022.121702.
573 [51] Xiaowen Zhang, Xin Zhang, Helei Liu, Wensheng Li, Min Xiao, Hongxia Gao, Zhiwu Lian. Reduction of
574 energy requirement of CO_2 desorption from a rich CO_2-loaded MEA solution by using solid acid catalysts.
575 Applied Energy 202 (2017) 673-684. http://dx.doi.org/10.1016/j.apenergy.2017.05.135.
576 [52] Zain Bair, Ya Pang, Jia Li, Abdo Hezam, Paitoon Tontiwachwuthikul, Han Chen. Reducing energy requirements
577 and enhancing MEA-CO_2 desorption rates in amine solutions with KIT-6 nanostructures. Separation and
578 Purification Technology, 346 (2024) 127536. https://doi.org/10.1016/j.seppur.2024.127536.
579 [53] Ozge Yukse lOrhan, Asulal Hugul, Neslisah Ulus, Hulya Yavuz Ersan. Enhancing CO_2 desorption efficiency
580 with Non-Aqueous Catalyst-Enhanced Tri-Blendamines. Fuel 375 (2024) 132458.
581 https://doi.org/10.1016/j.fuel.2024.132458.
582 [54] Siming Chen, Linlin Chen, Lei Zhang. Improving CO_2 desorption performance in monoethanolamine solutions
583 by adding titanium pyrophosphate catalyst. Scientific Reports 14 (2024) 30220. https://doi.org/10.1038/s41598-

584 024-81814-z.
585 [55] Xiaowen Zhang, Helei Liu, Zhiwu Liang, Raphael Idem, Paitoon Tontiwachwuthikul, Mohammed Jaber Al-
586 Marri, Abdelbaki Benamor. Reducing energy consumption of CO_2 desorption in CO_2-loaded aqueous amine
587 solution using Al_2O_3/HZSM-5 bifunctional catalysts. Applied Energy 229 (2018) 562-576.
588 https://doi.org/10.1016/j.apenergy.2018.07.035.
589 [56] Huancong Shi, Abdulaziz Naami, Raphael Idem, Paitoon Tontiwachwuthikul. Catalytic and noncatalytic solvent
590 regeneration during absorption-based CO_2 capture with single and blended reactive amine solvents.
591 International Journal of Greenhouse Gas Control, 26 (2014) 39-50.
592 http://dx.doi.org/10.1016/j.ijggc.2014.04.007.
593 [57] Xiayi Hu, Qian Yu, Yuanyuan Cui, Juntao Huang, Elenica Shiko, Yefeng Zhou, Zhaogang Zeng, Yang Liu and
594 Rui Zhang. Toward Solvent Development for Industrial CO_2 Capture by Optimizing the Catalyst-Amine
595 Formulation for Lower Energy Consumption in the Solvent Regeneration Process. Energy & Fuels, 33 (2019)
596 11507-11515. https://doi.org/10.1021/acs.energyfuels.9b02874.
597 [58] Dong Ye, Runxian Wang, Xiaoxiang Wang, Xin Liu, Hui Liu, Haining Wang. Improvement in the Hg^0 removal
598 performance of CeO_2 by modifying with CuO. Applied Surface Science, 579 (2022) 152200.
599 https://doi.org/10.1016/j.apsusc.2021.152200.
600 [59] Long Ji, Jiabi Li, Rongrong Zhai, Jinyi Wang, Xiaolong Wang, Shuiping Yan, and Ming Hua. Metal
601 Oxyhydroxide Catalysts Promoted CO_2 Absorption and Desorption in Amine-Based Carbon Capture: A
602 Feasibility Study. ACS Omega, 7 (2022) 44620-44630. https://doi.org/10.1021/acsomega.2c02851.